JES Focus Issue of Selected Papers from IMLB 2018

Self-Discharge Behavior of Lithium-Sulfur Batteries at Different Electrolyte/Sulfur Ratios

Chao Shen,[1,2] Jianxin Xie,[3,4] Mei Zhang,[3,4] Petru Andrei,[1,2] Mary Hendrickson,[5] Edward J. Plichta,[5] and Jim P. Zheng[1,2,6,*,z]

[1]*Department of Electrical and Computer Engineering, Florida A&M University and Florida State University, Tallahassee, Florida 32310, USA*
[2]*Aero-Propulsion, Mechatronics and Energy Center, Florida State University, Tallahassee, Florida 32310, USA*
[3]*Department of Industrial and Manufacturing Engineering, Florida A&M University and Florida State University, Tallahassee, Florida 32310, USA*
[4]*High-Performance Materials Institute, Florida State University, Tallahassee, Florida 32310, USA*
[5]*Army Power Division, RDER-CCA, Aberdeen Proving Ground, Maryland, USA*
[6]*Center for Advanced Power Systems, Florida State University, Tallahassee, Florida 32310, USA*

The commercialization of lithium sulfur (Li-S) batteries is hindered by their poor cycling performance, including fast capacity fade, low Coulombic efficiency, and high self-discharge rate. The static electrochemical stability of Li-S batteries, which is usually described in terms of their self-discharge properties, was much less studied compared to the dynamic electrochemical stability under continuous cycling. In this article, a set of experiments designed to understand the correlation between the self-discharge process and various operational conditions were made by using freestanding carbon nanotube foams as cathodes. We found a strong dependence of the self-discharge rate on the depth of discharge and on the electrolyte/sulfur ratio. We show that the effects of the self-discharge on the subsequent discharge capacities of Li-S cells are closely related to the type and concentration of lithium polysulfide species in the electrolyte and their interaction with the Li anode. This relation is analyzed in detail in this article, showing that one should pay special attention to the state-of-charge during self-discharge and the other operational conditions in order to improve the cyclability and capacity of Li-S batteries. In addition, we also highlight the importance of an efficient anode protection to improve the static electrochemical stability of these batteries.

 [DOI: 10.1149/2.0461903jes]

Manuscript submitted November 19, 2018; revised manuscript received December 21, 2018. Published January 2, 2019. *This paper is part of the JES Focus Issue of Selected Papers from IMLB 2018.*

Due to their high theoretical capacity, low cost, and environmental friendliness, lithium-sulfur (Li-S) batteries are promising candidates to replace traditional Li-ion batteries (LIBs) as the next-generation energy storage device.[1–3] The theoretical capacity of the sulfur cathode is 1672 mAh g^{-1} and, when assembled with a Li metal anode, the total specific energy of Li-S batteries is 3–5 folds higher than that of LIBs. For this reason, Li-S batteries are attractive in various applications that require high energy density, such as in electric vehicles, unmanned aerial devices, and portable electronics.

There is much research on the dynamic electrochemical stability of Li-S batteries, in which the cells are continuously discharged and charged at a given rate.[4–8] However, there are much fewer studies of the static electrochemical stability of these batteries, which is mainly described by the long-term self-discharge properties. Since the long-term self-discharge rate of Li-S batteries is much higher than in conventional LIBs and it causes significant capacity fade and even cell failure,[9] understanding and improving the static electrochemical stability during cell resting remains a huge challenge that needs considerably more research efforts.

It is generally believed that the high self-discharge rate of Li-S batteries is due to the diffusion and reactions of lithium polysulfide (LiPS) at the anode. The LiPS species are soluble in ether-based electrolytes and the electrolytes function as "catholytes" after the reduction of sulfur.[10] During the resting period, the diffusing polysulfides migrate toward the separator, reach the Li-metal anode, and undergo chemical reductions. Depending on the final products of these reactions, the capacity loss can be either recoverable or irrecoverable. For instance, when insoluble Li_2S_2/Li_2S mixtures are formed as a result of anode reactions, these mixtures precipitate and induce a passivation layer on the Li metal surface, causing active material loss and decreased cycle life. Many researchers have proposed different solutions for reducing the self-discharge rate of Li-S batteries, either by optimizing the electrolyte,[11–13] the cathodes,[14–17] and the separators,[18–22] or by designing new cell configurations.[23] Despite these efforts, the self-discharge properties were much less studied compared to the dynamic cycling efficiency and stability of Li-S batteries. Moreover, most current studies use Li-S cells with low or medium sulfur loadings, in which the electrolyte/sulfur (E/S) ratio is relatively high and there are very few studies that look at the self-discharge properties in batteries with low E/S ratios.

In this paper, we use freestanding carbon nanotube (CNT) foam cathodes to make Li-S batteries and study their self-discharge properties. Two different sulfur loadings, one with a medium sulfur loading (2 mg cm^{-2}, corresponding to an E/S ratio of 16 ml g^{-1}) that is often used in the published literature and one with a high sulfur loading (6.3 mg cm^{-2}, corresponding to an E/S ratio of 5 ml g^{-1}) that is adequate for practical applications, are studied and compared for their self-discharge behavior.

Experimental

Material preparation and characterization.—Sulfur, 1,2-dimethoxyethane (DME), 1,3-dioxolane (DOL), bis (trifluoromethane)sulfonimide (LiTFSI), and $LiNO_3$ were purchased from Sigma-Aldrich. The synthesized CNT foams containing CNTs (General Nano) with an average diameter of 10 nm and a length of 2 mm were assembled in a freestanding three-dimensional conductive network using the method presented in previous papers.[10,24] The C/S composite cathodes were made by infiltrating sulfur into the CNT foams via the melt diffusion method. Sulfur powder was placed on the surface of the CNT foam uniformly and then heated and melted into the CNT foam with a hot plate set at 158°C. Two types of cathodes, one with a high E/S ratio and the other one with a low E/S ratio were made using the two sulfur loadings mentioned above. The carbon density in each cell was 1.2 mg cm^{-2} and electrolyte volume

*Electrochemical Society Member.
[z]E-mail: zheng@eng.famu.fsu.edu

was 40 µl. Scanning electron microscopy (SEM, JEOL-JSM7401F, 10 kV) was used to characterize the morphology of the CNT foam cathodes before and after sulfur infiltration.

Electrochemical characterization.—The electrolyte used for coin cell assembly was composed of 1 M LiTFSI and 0.2 M $LiNO_3$ in DME:DOL (1:1 v:v) for the cells with a high E/S ratio, and 0.5 M LiTFSI and 0.5 M $LiNO_3$ in DME:DOL (1:1 v:v) for the cells with a low E/S ratio. The cathodes were assembled with Celgard 2400 separators and Li foil anodes (MTI) into CR2032-type coin cells. The galvanostatic cycling measurements were performed using a Neware multichannel battery cycler at room temperature. The electrochemical impedance spectrum (EIS) of the cells was recorded from 1 Hz to 1 MHz, at open circuit potential, using a frequency response analyzer (Gamry Instruments, Reference 3000) with an AC voltage amplitude of 10 mV.

The same type of self-discharge experiments was conducted for cells with both the high and low E/S ratio. For each E/S ratio, we made four identical cells that were discharged and charged for 50 cycles. The first three cells were first discharged and charged for 10 normal cycles (1.8–2.8 V) for initial stabilization. On the 11th discharge cycle, the discharge of each cell was stopped at different DODs and set to rest for 3 days, as follows:

Cell A: the first cell was set to rest at the beginning of the 11^{th} discharge cycle (i.e. immediately after the 10^{th} charge).

Cell B: the second cell was set to rest at the point on the discharge curve where the cell voltage was equal to 2.1 V.

Cell C: the third cell was set to rest at the midpoint of the lower plateau.

After resting, the three cells were discharged and charged again for another 40 cycles. Finally, the fourth cell (Cell D) was galvanostatically discharged and charged continuously for 50 cycles (1.8–2.8 V). The discharge and charge rates were 0.33 C for the cells with a high E/S ratio and 0.04 C for the cells with a low E/S ratio.

The results of the batteries that were left to self-discharge (cell A, cell B, and cell C) were compared to the results of the battery that was subject to continuous cycling without resting (cell D).

Quantification of self-discharge behavior.—The self-discharge behavior was quantified based on the previously presented methodology.[25] The total capacity loss after resting (C_{tot}) was divided into two components: the irrecoverable capacity loss (C_{ir}) and the recoverable capacity loss (C_r):

$$C_{tot}=C_{ir}+C_r \quad [1]$$

where all the terms are normalized to the capacity of the battery at the 10^{th} cycle and expressed in percentages as show in Fig. 1. The irrecoverable capacity loss was computed as

$$C_{ir}=100\% - Q_{max} \quad [2]$$

where Q_{max} is the maximum discharge capacity after the 10^{th} cycle (expressed in %). The specific capacity measured from the initial state to the oversaturation point (i.e. the voltage dip point) is denoted by Q_1 and the specific capacity from the oversaturation point until the death of the battery by Q_2 (see the inset in Fig. 1).

Results and Discussion

The SEM analysis of our cathodes shows that the sulfur is uniformly distributed on the surface of CNTs (see Fig. S1 in Supplementary Material). The self-discharge effects induced by the cathode current collector,[12] can be neglected in our freestanding cathode structure, so we can focus solely on the effects of the polysulfide diffusion. Next, we present results for the self-discharge properties of Li-S batteries at high and low E/S ratios. As we will see, the batteries present significantly different self-discharge characteristics in the two cases.

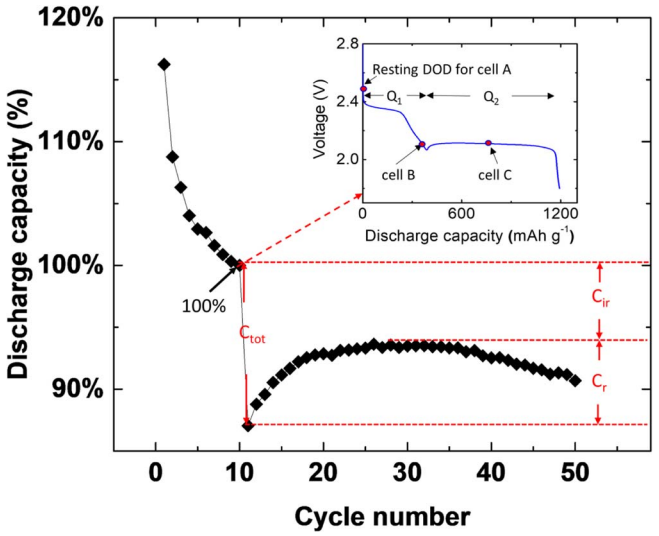

Figure 1. Illustration of self-discharge behavior quantification.

Self-discharge behavior at a high E/S ratio.—The discharge capacity of the four batteries with a high E/S ratio is plotted in Fig. 2a as a function of the cycle number. The specific capacity during the first cycle is 1205 ± 40 mAh g^{-1} for all the batteries fabricated in this study. The batteries also exhibit reasonably similar cycling performance during the first 10 cycles. However, during the 11^{th} cycle the four cells behave quite differently. The battery that is self-discharged at the end of the 10^{th} charge cycle (cell A) has the highest drop of the discharge capacity during the 11^{th} cycle, however this loss is almost entirely recovered during the 12^{th} cycle and $C_{tot} \approx C_r$. Resting the cell at 2.1 V (cell B), causes an irreversible drop of the discharge capacity. Finally, for cell C, both C_{ir} and C_r are relatively small. The components of the capacity loss were calculated for each battery using Equations 1 and 2 and are shown in Fig. 2b. Next, we analyze the mechanism of the self-discharge for each cell, separately.

The discharge and charge curves of cell A during the 10^{th} and 11^{th} cycle are represented in Fig. 2c. On the one hand, we observe that the starting voltage after resting during cycle 11 is significantly lower than that in cycle 10 and, as a result, the upper plateau capacity Q_1 decreased to almost zero, which is the major cause for the capacity loss, C_{tot}. On the other hand, there is no observable change in the lower plateau capacity Q_2 and after the recharge in cycle 11, the cell recovered almost the entire capacity. The above phenomena indicate that the major active material in the cell has transferred from elemental sulfur to lower-order LiPS (e.g., Li_2S_4) during resting. A possible reason is that the cell was not fully charged in cycle 10, leaving a small portion of soluble LiPS in the electrolyte. During the rest, comproportionation reactions promoted the dissolution of elemental sulfur into the liquid phase, which could trigger the redox shuttle effect

$$S + Li_2S_x \rightarrow Li_2S_y,\ x < y \quad [3]$$

$$Li + Li_2S_y \rightarrow Li_2S_z,\ y > z \geq 4 \quad [4]$$

Note that the soluble Li_2S_z can still be recovered during the following cycle. To confirm this assumption, we conducted two additional tests. First, we assembled a fresh cell and set it to rest immediately after assembly, without performing any initial cycles. In this condition, the fresh electrolyte contains a minimum amount of LiPS and the major species in the cell is elemental sulfur. During the rest, the open circuit voltage (OCV) shows little variation and the discharge specific capacity after resting shows a marginal change. Since the solubility of sulfur in the electrolyte is extremely low,[26] the slow sulfur dissolution into the electrolyte alone cannot cause significant self-discharge during the three-day resting period. This result is in agreement with other

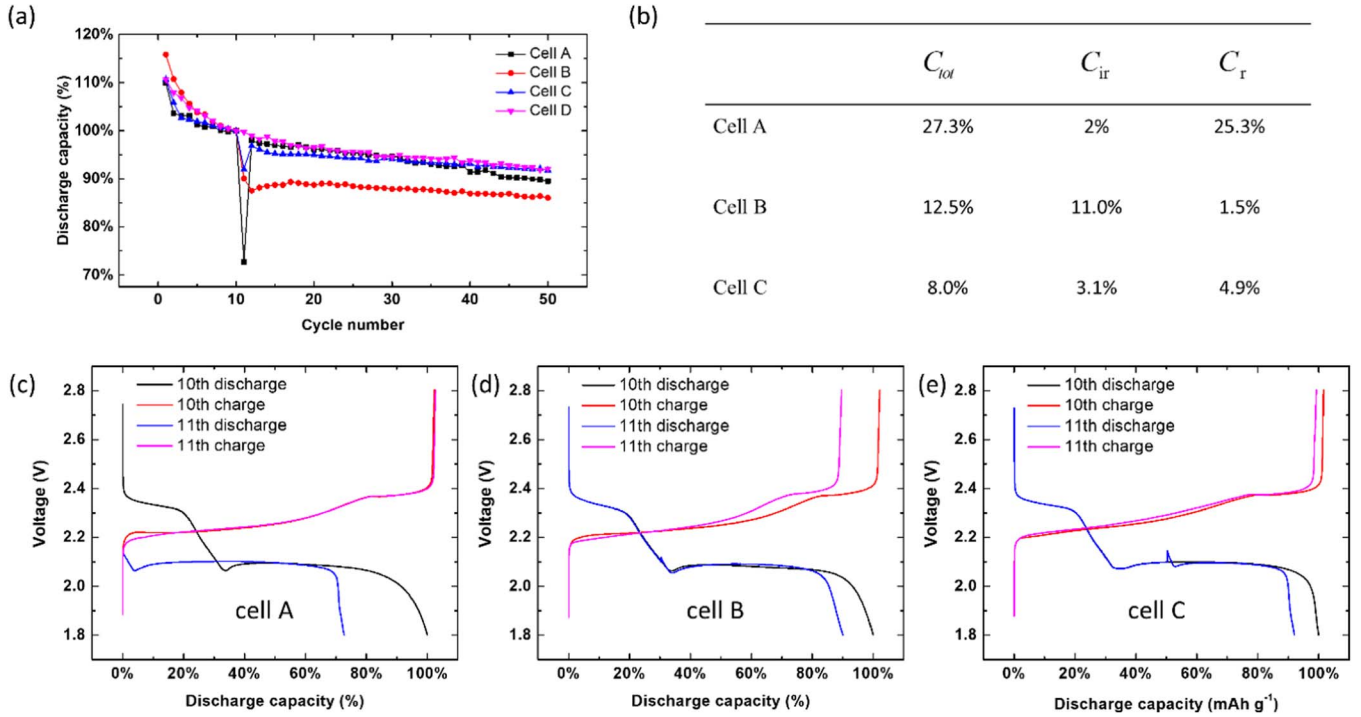

	C_{tot}	C_{ir}	C_r
Cell A	27.3%	2%	25.3%
Cell B	12.5%	11.0%	1.5%
Cell C	8.0%	3.1%	4.9%

Figure 2. Self-discharge behavior of Li-S cells at 0.33 C with a sulfur loading of 2 mg cm^{-2} and an E/S ratio of 16 ml g^{-1}. (a) Cycling performance of Li-S cells rested at different DODs. (b) Calculated self-discharge capacity loss for the three cells. (c) Voltage profiles for cell A. (d) Voltage profiles for cell B. (e) Voltage profiles for cell C.

publications in the literature showing that fresh Li-S batteries have better static electrochemical stability compared to cycled ones.[11,19,20] It is very likely that after cycling, LiPS promotes sulfur dissolution through Reaction 3.

Secondly, we repeated the self-discharge test but, at the end of cycle 10, after charging the battery at constant current (CC), we added a constant voltage (CV) charge to promote the further conversion of LiPS to sulfur (CC-CV). The corresponding voltage evolution and cycling performance is summarized in Fig. 3. Despite the fact that the charge capacity is only slightly increased due to the additional CV charge (see the red circle in Fig. 3a), the majority of the upper plateau is maintained in the voltage profile in cycle 11. As seen in Fig. 3b, after the CC-CV charge, the OCV decays much slower, while the voltage evolution of the cell after the CC charge resembles the typical upper plateau of the voltage profile in Li-S batteries, indicating that the cell was self-discharged to about 25% DOD and the majority of sulfur species is lower-order LiPS. As a result, C_{tot} is much reduced for the cell charged at CC-CV in cycle 10 (see Fig. 3c). The above results demonstrate that the interplay between sulfur and LiPS causes the large reversible loss C_r, when resting the cell at OCV. Therefore, to improve the static stability of the batteries at the fully charge state, it is necessary to ensure the batteries contain a minimum amount of LiPS in the electrolyte during resting.

As mentioned above, resting the cell at 2.1 V causes the largest irrecoverable loss C_{ir} (see Fig. 2d). To investigate the reason for the different self-discharge behavior between cell A and cell B, we compute the concentration of different LiPS species in the electrolyte as a function of discharge capacity using the previous reported model.[27] As seen in Fig. 4, the total concentration of LiPS in the electrolyte reaches its maxima in the dip point of the voltage profile (near 2.1 V), which agrees well with other reported experimental observations.[18,28] Therefore, one effective way to evaluate the self-discharge behavior of the cells with high LiPS concentrations is to rest the cells at 2.1 V and observe the difference between the discharge capacity before and after the resting period.[15] In this case, the major species in the electrolyte is S_4^{2-} (see Fig. 4) and, consequently, the chemical Reaction 5 could cause the precipitation of immobile Li_2S_2/Li_2S rather than soluble LiPS intermediates on the Li surface

$$Li + Li_2S_y \rightarrow Li_2S_z,\ y \geq 4 > z \qquad [5]$$

This precipitate becomes "dead" sulfur residual and cannot be recovered during the following cycles.

To further confirm this assumption, we fabricated cells with different $LiNO_3$ concentrations and subject them to the same cycling performance as cell B. The results of the discharge capacities of these cells are represented in Fig. 5. $LiNO_3$ is known to be an effective electrolyte additive that passivates the Li anode from side reactions with LiPS.[12,29–31] Therefore, it is expected that the increased $LiNO_3$ concentration can reduce C_{ir} caused by resting. As expected, the cell with an increased concentration of 0.4 M $LiNO_3$ shows the smallest C_{ir} due to the better protection of Li anode. Interestingly, the cell with 0 M $LiNO_3$ could be cycled before the resting but, due to the severe side reactions between LiPS and Li anode, the Coulombic efficiency is significantly lower (see Fig. S2 in Supplementary Material) resulting in a large C_{tot} of 33.2%. This cell failed completely during the next charging cycle. This phenomenon highlights once again the importance of static stability of Li-S batteries. Although an unprotected Li anode can still be cycled dynamically, the chemical reactions severely affect the cycle life of the cell after resting.[32–34]

Cell C exhibits an improved static stability when operated within the lower plateau (see Fig. 2). As shown in Fig. 4, the LiPS concentration in the electrolyte is continuously reduced due to the precipitation of Li_2S during the discharge on the lower plateau. Therefore, the unfavorable reactions on the anode side are significantly reduced in cell C, which results in a smaller capacity loss (see Fig. 2e).

Self-discharge behavior at a low E/S ratio.—Another set of four identical Li-S cells was made using a low E/S ratio and subject to the same testing methodology as the cells with a high E/S ratio. To be able to perform a direct comparison between the cells with low and high E/S ratios the cells are also labeled as cell A, B, C, and D. To improve the cycle stability under the lean electrolyte condition and ensure that

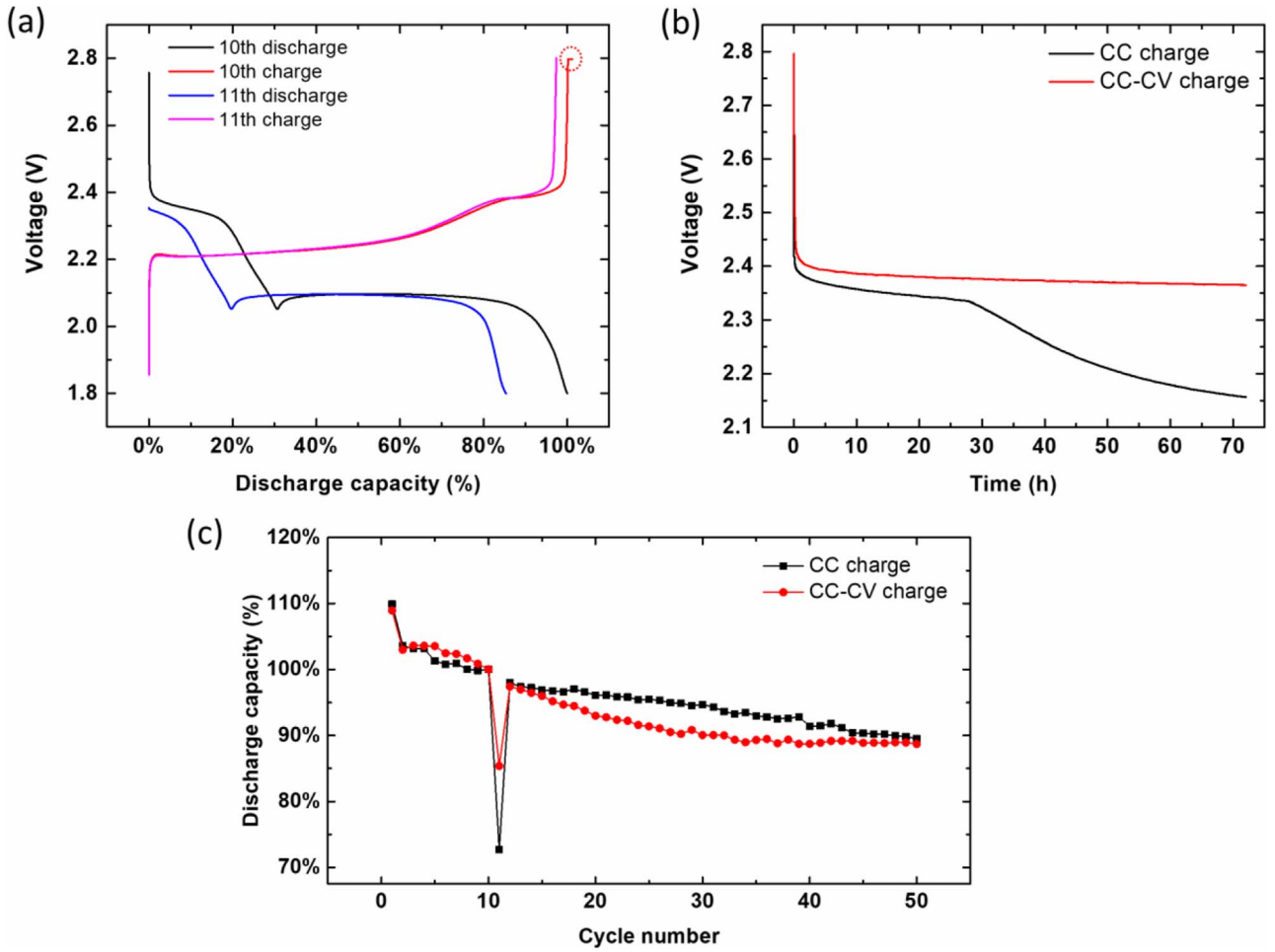

Figure 3. (a) Voltage profiles of a Li-S cell that has a CC-CV charging during cycle 10 and CC charging during all the other cycles. (b) Comparison between the OCV of cell A and the OCV of the Li-S cell with CC-CV charging during cycle 10, during resting. (c) Comparison between the cycling performance of cell A and the Li-S cell with CC-CV charging during cycle 10.

there are enough species to form the solid electrolyte interphase (SEI) on the anode surface,[5,35–38] we slightly increased the concentration of $LiNO_3$ to 0.5 M and decreased the concentration of LiTFSI to 0.5 M in the DME:DOL (1:1 v:v) solvent.

The self-discharge behavior of the cells with a low E/S ratio is summarized in Fig. 6. The average initial specific capacity is reduced to 423.7 ± 30 mAh g^{-1} for all four cells. Note that there is a huge capacity decay from the 1st to the 2nd cycle while, in the following initial cycles, the specific discharge capacity slowly increases until

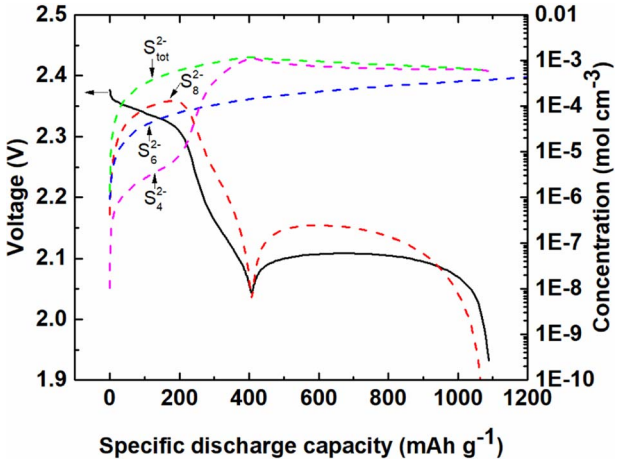

Figure 4. Calculated average concentration of polysulfide species as a function of specific discharge capacity. S_{tot}^{2-} denotes the total sulfur concentration in the electrolyte.

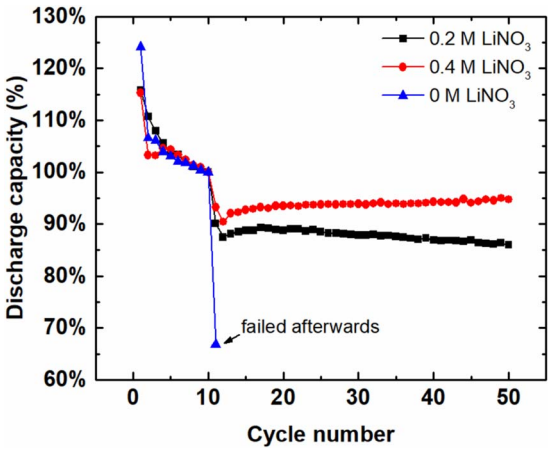

Figure 5. Cycling performance of Li-S cells with different $LiNO_3$ concentrations. The cells were continuously discharged and charged until cycle 10, when they were set to rest for 3 days.

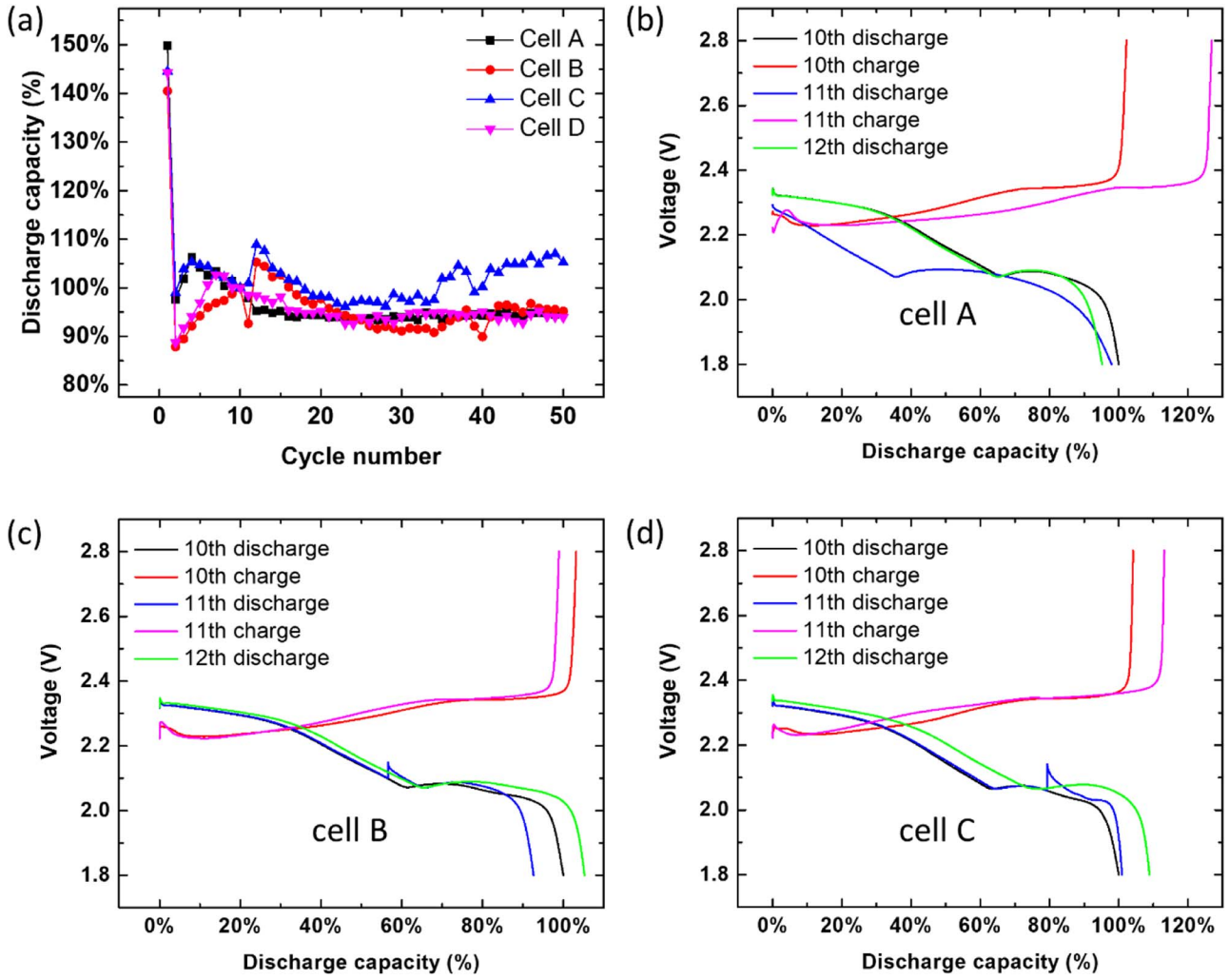

Figure 6. Self-discharge behavior of Li-S cells with a sulfur loading of 6.3 mg cm^{-2} and an E/S ratio of 5 ml g^{-1}, at 0.04 C. (a) Cycling performance of Li-S cells rested at different DODs. (b) Voltage profiles for cell A. (c) Voltage profiles for cell B. (d) Voltage profiles for cell C.

the equilibrium between the discharge and charge process is established. More importantly, by comparing these results with the ones in Fig. 2, one notice that there are significant differences between the self-discharge behavior of the batteries with a high E/S ratio and those with a low E/S ratio. In the case of the batteries with a low E/S ratio, there is no significant irreversible capacity loss C_{ir}. The voltage profile of cell A is significantly altered during cycle 11 (see Fig. 6b) but shows no significant change of the total discharge capacity. Somewhat unexpected, in the case of cells B and C, the discharge capacity shows a slight increase during cycle 12 (see Figs. 6c–6d). We also conducted the above test with electrolytes containing different $LiNO_3$ concentrations and despite their discharge capacity difference, the same phenomena were consistently observed. Next, we analyze the mechanism of the self-discharge for each cell, separately.

Although there is no significant capacity loss after resting cell A, the discharge curves of this cell change significantly from cycle 10 to cycle 11 (see Fig. 6b). This change is mostly given by the dramatic change of the Q_2/Q_1 ratio, which, coincidently, yields to a similar overall discharge capacity. After resting, capacity Q_1 decreases for the same reason as described in Self-discharge behavior at a high E/S ratio section. Due to a higher sulfur loading, the OCV drop and the corresponding drop in Q_1 are smaller. However, surprisingly, Q_2 increases more than twice after resting (cycle 11) than before resting (cycle 10). There are multiple reasons that can account for this phenomenon. First, after the resting period, the solid sulfur and possibly the $LiPS_{(S)}$ formed during cycling can slowly dissolve in the electrolyte, increasing the active surface area available for solid deposition during the discharge on the lower plateau. Secondly, some Li_2S nucleation seeds can form on the surface of the cathode during the resting period, which will facilitate the precipitation of Li_2S and increase the duration of the discharge on the lower plateau.[27]

In order to understand the physical processes occurring during the resting period, an in-situ EIS test was conducted before, during, and after resting. The EIS has been utilized before as a powerful diagnostic tool to investigate electrode/electrolyte interfaces during discharge and charge.[28,39–41] In this study, we also recorded the EIS evolution at equal intervals of time during the resting period. The voltage profiles and the measured EIS curves are plotted in Fig. 7. As one can see from this figure, the EIS curves at 2.1 V (P1) and 1.8 V (P2), before and after resting, are relatively similar. At 2.1 V, the charge-transfer resistance, computed as the diameter of the semi-circle on the corresponding EIS curve, decreases only slightly from 22.9 Ω to 18.2 Ω, which indicates that the surface coverage condition has not changed much while discharging the cell from the fully discharged state to 2.1 V. Therefore, it is likely that other effects are accountable for the increase of Q_2.

In addition, the decreased charge-transfer resistance at P0 after resting is due to the decreased surface coverage, which is illustrated in Figs. 7c–7d. Upon resting from R0 to R1, the dissolved sulfur species significantly reduce the charge-transfer resistance. Afterwards, the

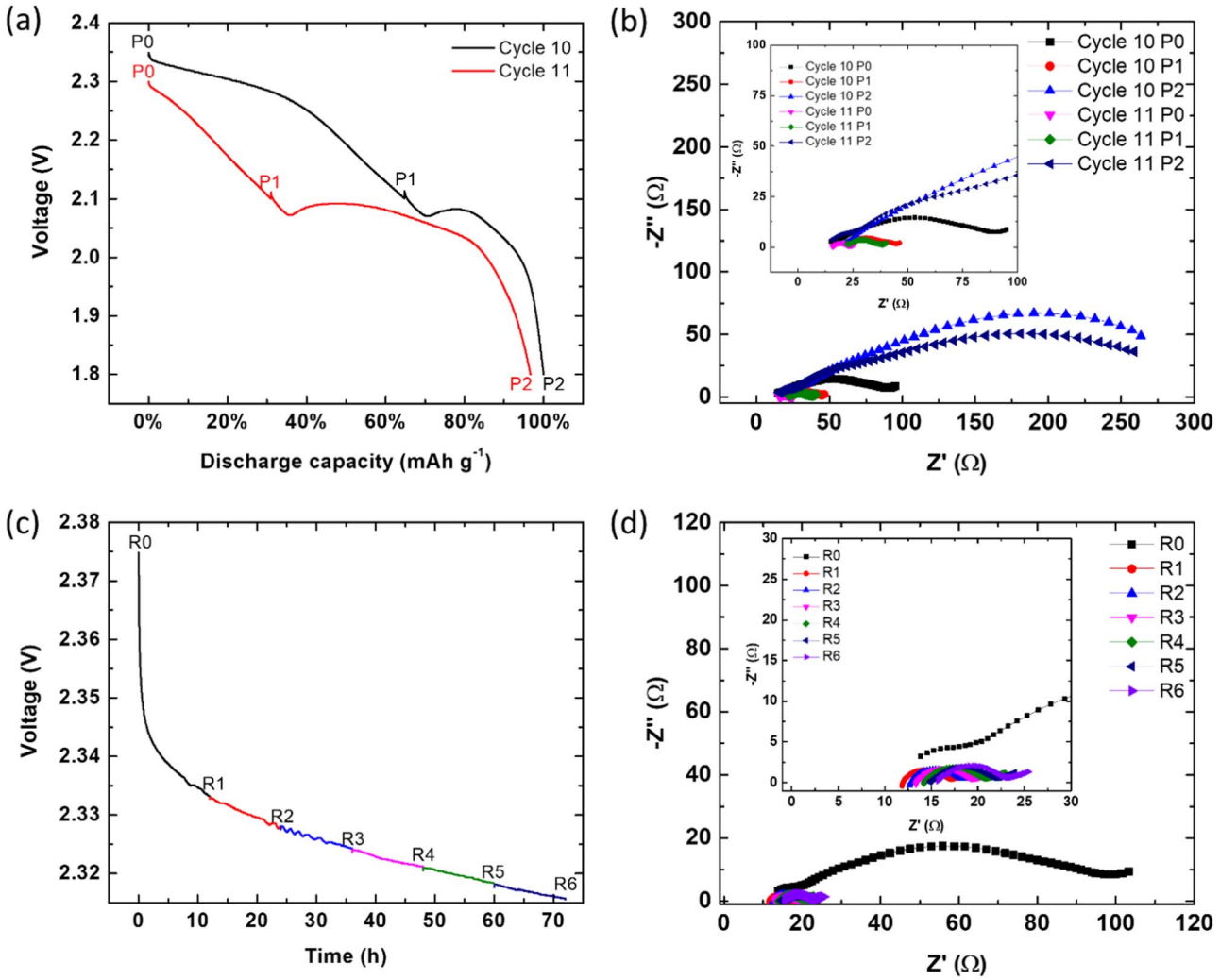

Figure 7. In-situ EIS measurement of cell A before and after resting. (a) Discharge profiles of Li-S cells before (Cycle 10) and after resting (cycle 11). (b) EIS curves of the Li-S cell before and after resting. (c) OCV evolution of the Li-S cell during resting. (d) EIS curves of the Li-S cell during resting.

electrolyte conductivity decreases gradually due to self-discharge on the upper plateau and the EIS curves continuously shift to the right. However, this shift is relatively negligible compared to the change of the EIS from R0 to R1.

We believe that the formation of nucleation seeds during the resting period is the major reason for the increased capacity of the lower plateau Q_2 observed from cycle 10 to cycle 11. This assumption is in agreement with the theoretical model presented in our previous work,[27] which shows that the deposition of Li_2S follows a dissolution-precipitation mechanism. According to this model, after the formation of the initial nuclei seeds, the Li_2S species formed on the surface of the cathode diffuse in the electrolyte and precipitate on the surface of the existing seeds, away from the surface of the carbon. The driving force of the initial nucleation process (i.e. the formation of the solid seeds) is the oversaturation of Li_2S at the surface of the carbon. During cycle 10, nucleation seeds are formed at the onset of the lower plateau, when the electrolyte is highly oversaturated (see Fig. 8). Once the deposition starts, the densely packed solid Li_2S quickly passivates the cathode surface and terminates the electrochemical reactions. During cycle 11, since the E/S ratio is low, a small number of Li_2S seeds can form on the surface of cathode during the resting period and serve as growing centers for the solid deposition. These sparsely packed seeds reduce the surface oversaturation and allow for a longitudinal growth of the Li_2S during the lower plateau. In contrast, in the case of high E/S ratios, the concentration of the LiPS is relatively small during the resting period and the Li_2S seeds cannot form on the surface of cathode. This is the reason why Q_2 does not change much from cycle 10 to cycle 11 in the case of the cell with a high E/S ratio (see Fig. 2c), however, it increases significantly in the case of the cell with a low E/S ratio. In cycle 12, the seeds that were formed during cycle 11 are charged back and no longer exist, and the voltage profile recovers its initial shape (see Fig. 6b).

The self-discharge characteristics of cells B and C are rather similar. The discharge capacity increases in cycle 12 mainly because of an increase of the capacity of its upper plateau Q_1 (see Figs. 6c–6d). This phenomenon is somewhat counterintuitive and is due to reactions at the anode side. During the continuous cycling of the cells, some higher-order LiPS are "trapped" at the anode side due to their limited mobility in the highly concentered electrolyte. However, they can slowly diffuse back to the cathode side while resting the cell at 2.1 V or during the resting on the lower plateau. As a result, they can be further reduced after the resting period, which results in a small increase of Q_1 during cycle 12.

Conclusions

The discharge and charge characteristics of the cells analyzed in this work strongly depend on the E/S ratio and DOD during the resting period. At a high E/S ratio, the self-discharge behavior is

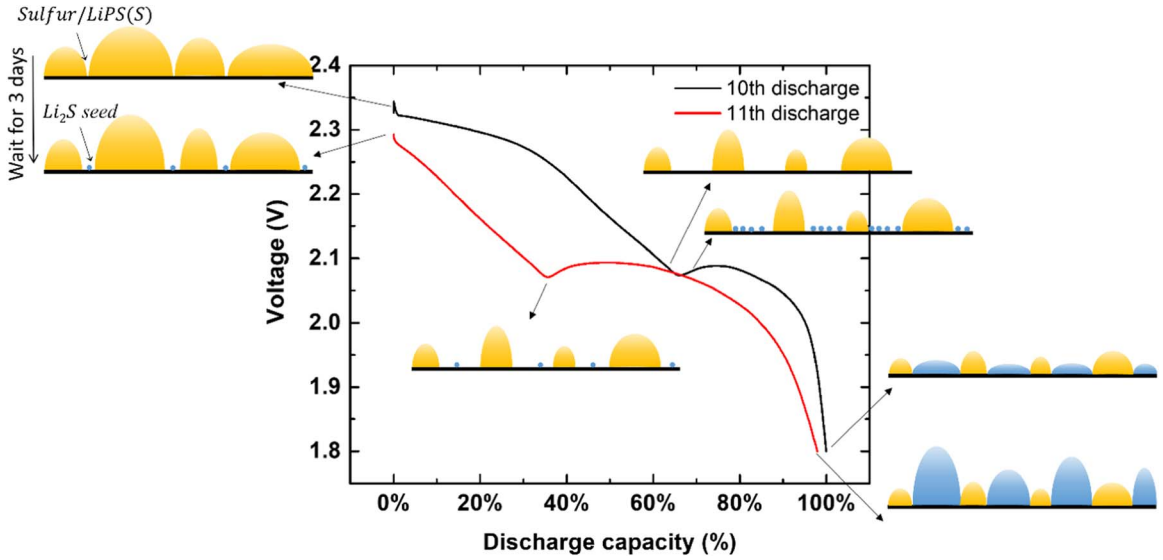

Figure 8. Nucleation and precipitation process for Li-S cell A with a low E/S ratio, before and after resting.

more severe, while at low E/S ratio the cells exhibit an improved static electrochemical stability.

Our analysis shows that the effects of self-discharge on the subsequent cycles are related to the Li anode passivation and LiPS diffusion rates at the different E/S ratios. For instance, as indicated in this work and also reported by other research papers,[42–44] the characteristics of the anode SEI layer strongly depend on the type and concentration of LiPS species. In the case of low E/S ratios, once the SEI layer is completely formed, it will decrease the reaction rates between LiPS and the Li anode, and the self-discharge rate of the battery will be significantly reduced. In addition, since the self-discharge phenomena are closely related to the diffusion of LiPS, which is a time- and concentration-dependent process, parameters such as idling time and electrolyte volume significantly affect the observed phenomena. Therefore, when comparing the effects of self-discharge in different cells, one needs to pay considerable attention to the operational conditions of these cells, in particular to the state-of-charge and LiPS concentration during resting.

More research progress needs to be made to achieve an effective stabilization and immobilization of LiPS from free diffusion to the Li anode in order to improve the cycle performance and reduce the self-discharge rate of Li-S batteries.[32,45–49] In addition, the investigation of Li anode in Li-S batteries deserves much more attention. As revealed in a 2018 review paper, 64% of the papers published in the literature on Li-S batteries focus on the sulfur cathode, while only 2% on the Li anode.[50] Our work shows that it is of primary importance to understand the surface chemistry of the Li anode in the presence of LiPS species and develop effective protection strategies.

Finally, advanced quantitative characterization methods are needed to monitor the evolution of sulfur species during the resting period, especially in cells with lean electrolyte. Special attention should be paid to determine the role of multiple disproportionation and comproportionation reactions in the battery performance, which can play an important role not only during the continuous cycling but also during the resting period. The accurate mathematical modeling of the self-discharge phenomena can also help us understand the fundamental processes that take place during self-discharge.[51–53]

Acknowledgments

This work was supported by US Army Power Division under contract No. GTS-S-15-014 and by the National Science Foundation under grant No. 1609860.

ORCID

Chao Shen https://orcid.org/0000-0001-5270-4841
Jim P. Zheng https://orcid.org/0000-0003-2689-0067

References

1. H. Wu, L. Xia, J. Ren, Q. Zheng, F. Xie, W. Jie, C. Xu, and D. Lin, *Electrochim. Acta*, **278**, 83 (2018).
2. Z. Chen, J. Zhou, Y. Guo, C. Liang, J. Yang, J. Wang, and Y. Nuli, *Electrochim. Acta*, **282**, 555 (2018).
3. D. Zheng, G. Wang, D. Liu, J. B. Harris, T. Ding, J. Si, D. Qu, X. Yang, and D. Qu, *Electrochim. Acta*, **282**, 687 (2018).
4. M. Marinescu, L. O'Neill, T. Zhang, S. Walus, T. E. Wilson, and G. J. Offer, *J. Electrochem. Soc.*, **165**, A6107 (2018).
5. H. Schneider, T. Weiß, C. Scordilis-Kelley, J. Maeyer, K. Leitner, H.-J. Peng, R. Schmidt, and J. Tomforde, *Electrochim. Acta*, **243**, 26 (2017).
6. S. Waluś, C. Barchasz, R. Bouchet, J. C. Leprêtre, J. F. Colin, J. F. Martin, E. Elkaïm, C. Baehtz, and F. Alloin, *Adv. Energy Mater.*, **5**, 1 (2015).
7. H. Wang, N. Sa, M. He, X. Liang, L. F. Nazar, M. Balasubramanian, K. G. Gallagher, and B. Key, *J. Phys. Chem. C*, **121**, 6011 (2017).
8. E. V. Kuzmina, E. V. Karaseva, D. V. Kolosnitsyn, L. V. Sheina, N. V. Shakirova, and V. S. Kolosnitsyn, *J. Power Sources*, **400**, 511 (2018).
9. C. Barchasz, B. Chavillon, L. Boutafa, and E. Mayousse, *Electrochim. Acta*, (2018).
10. C. Shen, J. Xie, M. Zhang, P. Andrei, M. Hendrickson, E. J. Plichta, and J. P. Zheng, *Electrochim. Acta*, **248**, 90 (2017).
11. W. Li, Y. Pang, T. Zhu, Y. Wang, and Y. Xia, *Solid State Ionics*, **318**, 82 (2018).
12. M. Kazazi, M. R. Vaezi, and A. Kazemzadeh, *Ionics (Kiel).*, **20**, 1291 (2014).
13. L. Wang, J. Liu, S. Yuan, Y. Wang, and Y. Xia, *Energy Environ. Sci.*, **9**, 224 (2016).
14. Y. Pang, Y. Wen, W. Li, Y. Sun, T. Zhu, Y. Wang, and Y. Xia, *J. Mater. Chem. A*, **5**, 17926 (2017).
15. C. J. Hart, M. Cuisinier, X. Liang, D. Kundu, A. Garsuch, and L. F. Nazar, *Chem. Commun.*, **51**, 2308 (2015).
16. S.-H. H. Chung and A. Manthiram, *Adv. Mater.*, **30**, 1705951 (2018).
17. S. Chung, K. Lai, and A. Manthiram, **1805571**, 1 (2018).
18. K. Yang, L. Zhong, Y. Mo, R. Wen, M. Xiao, D. Han, S. Wang, and Y. Meng, *ACS Appl. Energy Mater.*, (2018).
19. S. H. Chung and A. Manthiram, *ACS Energy Lett.*, **2**, 1056 (2017).
20. S. H. Chung, P. Han, and A. Manthiram, *ACS Appl. Mater. Interfaces*, **9**, 20318 (2017).
21. J. Zhu, C. Chen, Y. Lu, J. Zang, M. Jiang, D. Kim, and X. Zhang, *Carbon N. Y.*, **101**, 272 (2016).
22. W. T. Xu, H. J. Peng, J. Q. Huang, C. Z. Zhao, X. B. Cheng, and Q. Zhang, *ChemSusChem*, **8**, 2892 (2015).
23. S.-H. Chung, C.-H. Chang, and A. Manthiram, *Energy Environ. Sci.*, **9**, 3188 (2016).
24. C. Shen, J. Xie, T. Liu, M. Zhang, P. Andrei, L. Dong, M. Hendrickson, E. J. Plichta, and J. P. Zheng, *J. Electrochem. Soc.*, **165**, A2833 (2018).
25. V. Knap, D.-I. Stroe, M. Swierczynski, R. Teodorescu, and E. Schaltz, *J. Electrochem. Soc.*, **163**, A911 (2016).
26. D. Zheng, X. Zhang, C. Li, M. E. McKinnon, R. G. Sadok, D. Qu, X. Yu, H.-S. Lee, X.-Q. Yang, and D. Qu, *J. Electrochem. Soc.*, **162**, A203 (2014).
27. P. Andrei, C. Shen, and J. P. Zheng, *Electrochim. Acta*, **284**, 469 (2018).
28. N. A. Canas, K. Hirose, B. Pascucci, N. Wagner, K. A. Friedrich, and R. Hiesgen, *Electrochim. Acta*, **97**, 42 (2013).

29. S. S. Zhang, *Electrochim. Acta*, **70**, 344 (2012).
30. S. S. Zhang, *Electrochim. Acta*, **97**, 226 (2013).
31. S. Xiong, K. Xie, Y. Diao, and X. Hong, *Electrochim. Acta*, **83**, 78 (2012).
32. Z. Cui, C. Zu, W. Zhou, A. Manthiram, and J. B. Goodenough, *Adv. Mater.*, 6926 (2016).
33. S. Evers and L. F. Nazar, *Acc. Chem. Res.*, **46**, 1135 (2013).
34. J. Sun, J. Liang, J. Liu, W. Shi, N. Sharma, W. Lv, R. Lv, Q. H. Yang, R. Amal, and D. W. Wang, *Energy Environ. Sci.*, **11**, 2509 (2018).
35. M. Agostini, J.-Y. Hwang, H. M. Kim, P. Bruni, S. Brutti, F. Croce, A. Matic, and Y.-K. Sun, *Adv. Energy Mater.*, **i**, 1801560 (2018).
36. Q. Wang, N. Yan, M. Wang, C. Qu, X. Yang, H. Zhang, X. Li, and H. Zhang, *ACS Appl. Mater. Interfaces*, **7**, 25002 (2015).
37. A. Jozwiuk, H. Sommer, J. Janek, and T. Brezesinski, *J. Power Sources*, **296**, 454 (2015).
38. K. Sun, A. K. Matarasso, R. M. Epler, X. Tong, D. Su, A. C. Marschilok, K. J. Takeuchi, E. S. Takeuchi, and H. Gan, *J. Electrochem. Soc.*, **165**, A416 (2018).
39. J. Conder, C. Villevieille, S. Trabesinger, P. Novák, L. Gubler, and R. Bouchet, *Electrochim. Acta*, **244**, 61 (2017).
40. J. Conder, C. Villevieille, S. Trabesinger, P. Novák, L. Gubler, and R. Bouchet, *Electrochim. Acta*, **255**, 379 (2017).
41. M. Li, Y. Zhang, Z. Bai, W. W. Liu, T. Liu, J. Gim, G. Jiang, Y. Yuan, D. Luo, K. Feng, R. S. Yassar, X. Wang, Z. Chen, and J. Lu, **1804271**, 1 (2018).
42. X.-B. Cheng, J.-Q. Huang, and Q. Zhang, *J. Electrochem. Soc.*, **165**, A6058 (2018).
43. W. Li, H. Yao, K. Yan, G. Zheng, Z. Liang, Y.-M. Chiang, and Y. Cui, *Nat. Commun.*, **6**, 7436 (2015).
44. C. Yan, X. B. Cheng, C. Z. Zhao, J. Q. Huang, S. T. Yang, and Q. Zhang, *J. Power Sources*, **327**, 212 (2016).
45. L. Jin, G. Li, B. Liu, Z. Li, J. Zheng, and J. P. Zheng, *J. Power Sources*, **355**, 147 (2017).
46. W. Yang, W. Yang, A. Song, L. Gao, G. Sun, and G. Shao, *J. Power Sources*, **348**, 175 (2017).
47. Y. X. Ren, T. S. Zhao, M. Liu, Y. K. Zeng, and H. R. Jiang, *J. Power Sources*, **361**, 203 (2017).
48. H. J. Peng, J. Q. Huang, X. Y. Liu, X. B. Cheng, W. T. Xu, C. Z. Zhao, F. Wei, and Q. Zhang, *J. Am. Chem. Soc.*, **139**, 8458 (2017).
49. C. Y. Fan, S. Y. Liu, H. H. Li, Y. H. Shi, H. F. H. C. Wang, H. F. H. C. Wang, H. Z. Sun, X. L. Wu, and J. P. Zhang, *J. Mater. Chem. A*, **5**, 11255 (2017).
50. T. Cleaver, P. Kovacik, M. Marinescu, T. Zhang, and G. Offer, *J. Electrochem. Soc.*, **165**, A6029 (2018).
51. S. M. Al-Mahmoud, J. W. Dibden, J. R. Owen, G. Denuault, and N. Garcia-Araez, *J. Power Sources*, **306**, 323 (2016).
52. V. Knap, D. I. Stroe, M. Swierczynski, R. Purkayastha, K. Propp, R. Teodorescu, and E. Schaltz, *J. Power Sources*, **336**, 325 (2016).
53. A. F. Hofmann, D. N. Fronczek, and W. G. Bessler, *J. Power Sources*, **259**, 300 (2014).